Electronic Supplementary Information

Tuning the NIR Downconversion Luminescence and Photothermal Conversion Efficiencies of $M\mathrm{Nd}_x\mathrm{Y}_{1-x}\mathrm{F}_4$ (*M* = Na, Li) Nanocrystals for Use in Anti-counterfeiting Labels with Opposite Displays

*Xiangyang Wu and Edwin K. L. Yeow**

Division of Chemistry and Biological Chemistry, School of Physical and Mathematical Sciences, Nanyang Technological University, 21 Nanyang Link, Singapore 637371

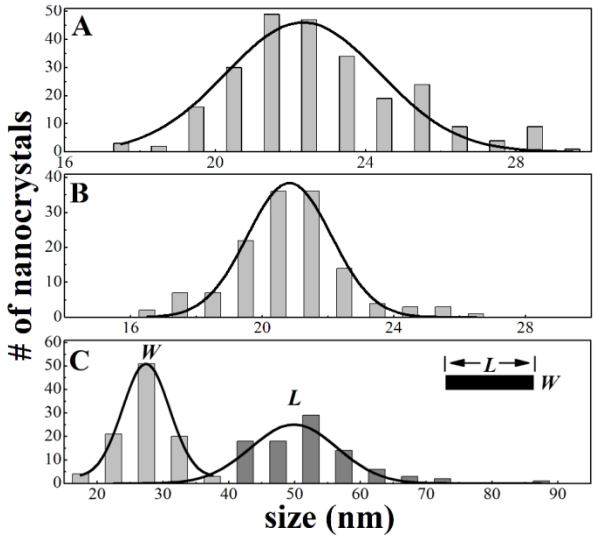

Fig. S1 Histograms of the size distribution of $NaNd_xY_{1-x}F_4$ nanocrystals for reaction time = 120 min; x = 3% (A), 20% (B) and 100% (C). The Gaussian fits shown give the average diameters of $NaNd_{0.03}Y_{0.97}F_4$ and $NaNd_{0.2}Y_{0.8}F_4$ nanoparticles to be 22.3 ± 4.1 and 20.8 ± 2.6 nm, respectively. The average length (L) and average width (W) of $NaNdF_4$ nanorods are 49.9 ± 14.4 and 27.4 ± 7.1 nm, respectively.

Growth dynamics of $NaNd_xY_{1-x}F_4$ nanocrystals

The growth mechanism of β-$NaNd_{0.03}Y_{0.97}F_4$ nanoparticles in Fig. 1A is studied by examining the TEM images and XRD patterns of nanocrystals prepared for various reaction times at 290 ^oC. At the start of the reaction, when the temperature first reaches 290 ^oC (reaction time t = 0 min), small irregular nanocrystals (average length ~ 4.5 nm) are formed (Fig. S2A and Fig. S3). The diffraction peaks in the corresponding XRD pattern match those of standard cubic phase α-$NaYF_4$ (JCPDS No. 77-2042) and NaF (JCPDS card no. 88-2299) (Fig. S2D). The latter is formed from the reaction: $NH_4F + NaOH \rightarrow NaF + NH_3 + H_2O$.

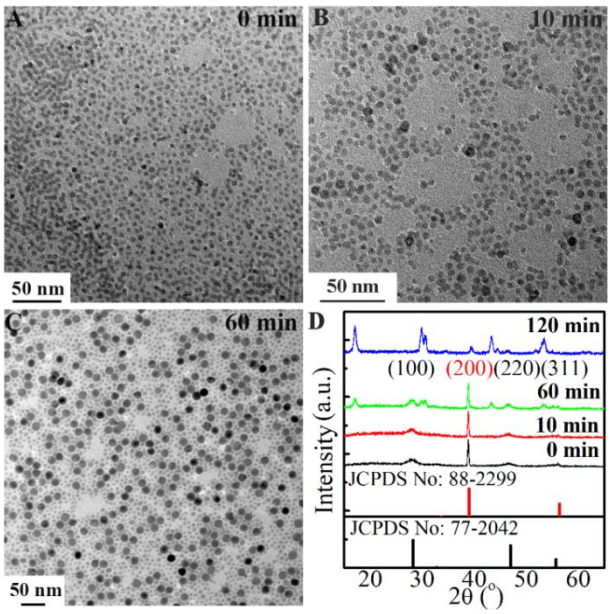

Fig. S2 (A-C) TEM images of $NaNd_{0.03}Y_{0.97}F_4$ nanocrystals obtained after different reaction times at 290 ^oC (A: 0 min, B: 10 min, and C: 60 min). (D) The corresponding XRD patterns (black: 0 min, red: 10 min, green: 60 min and blue: 120 min). The standard cards of cubic $NaYF_4$ (JCPDS No: 77-2042) and cubic NaF (JCPDS No: 88-2299) are shown. Lattice planes are labeled using different font colors (black: cubic $NaYF_4$ and red: cubic NaF). The XRD patterns are normalized with respect to the most intense peak.

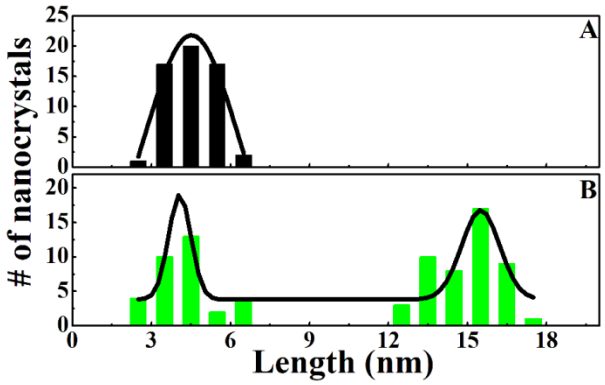

Fig. S3 Histograms of the size distribution of $NaNd_{0.03}Y_{0.97}F_4$ nanocrystals obtained at 290 °C for different reaction times (A: 0 min and B: 60 min). The Gaussian fit in A gives the average length of nanocrystals for t = 0 min to be 4.5 ± 3.5 nm. The Gaussian fits in B give the average diameters of the small and large nanoparticles formed for t = 60 min to be 4.1 ± 0.8 and 15.5 ± 1.4 nm, respectively.

When the reaction time is extended to t = 10 and 60 min, large spherical nanoparticles surrounded by smaller ones are seen (Fig. S2B and S2C), with the former increasing in size with reaction time. For an example, for t = 60 min, the group of small nanoparticles have an average diameter of 4.1 nm whereas the group of larger nanoparticles have an average diameter of 15.5 nm (Fig. S3). For t = 120 min, only spherical nanoparticles of average diameter = 22.3 nm are prepared (Fig. 1A).

The normalized XRD pattern for t = 10 min shows the presence of cubic phase α-$NaNd_{0.03}Y_{0.97}F_4$ nanocrystals (Fig. S2D). On the other hand, for t = 60 min, the co-existence of both α- and β-phase $NaNd_{0.03}Y_{0.97}$ nanoparticles are noted in the XRD pattern (Fig. S2D), and for t = 120 min, only β-phase nanoparticles are observed (Fig. S2D). Since NaF is only very slightly soluble in ethanol, the small amount of NaF removed during the nanocrystal precipitation process will be the same across all nanocrystals as the procedure is similar. From the un-normalized XRD pattern (Fig. S4), it is observed that the NaF peak for t = 60 min is less intense compared to the corresponding peak for t = 0 min. This indicates that NaF is being consumed in the production of the cubic phase nanocrystals. As the reaction progresses, the initially formed unstable α-$NaNd_{0.03}Y_{0.97}F_4$ nanocrystals undergo dissolution to monomers while facilitating the growth of β-

$NaNd_{0.03}Y_{0.97}F_4$ nanoparticles by redepositing onto them (*i.e.*, Ostwald ripening).[1] For t = 120 min, when only the hexagonal phase nanocrystals are found, we do not observe NaF (Fig. 1E).

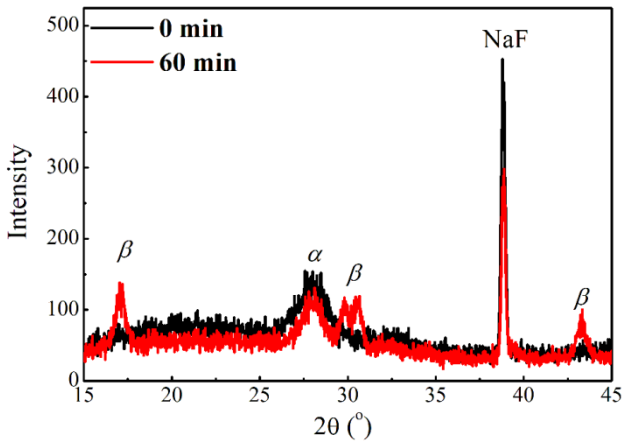

Fig. S4 Un-normalized XRD patterns of $NaNd_{0.03}Y_{0.97}F_4$ obtained at T = 290 ºC for t = 0 and 60 min. Diffraction peaks from cubic and hexagonal nanocrystals are labeled as 'α' and 'β'.

Shan and Ju have proposed that NaF plays a role in the nucleation of α– and β-$NaYF_4$ nanoparticles.[2] Furthermore, together with the monomers from the dissolution of α-$NaYF_4$ nanoparticles, unreacted NaF is further consumed during the growth of β-$NaYF_4$ nanoparticles.[2] Our results are in line with those of Wihelm *et al*. who also reported the presence of NaF at various stages during the synthesis of β-$NaYF_4$:Yb^{3+},Er^{3+} nanoparticles.[3] The authors observed the XRD diffraction peak of NaF during the nucleation of α-$NaYF_4$:Yb^{3+},Er^{3+} nanoparticles at early times and later when a mixture of α- and β-$NaYF_4$:Yb^{3+},Er^{3+} nanoparticles is present. The peak disappears when α–$NaYF_4$:Yb^{3+},Er^{3+} nanoparticles are fully converted to the hexagonal phase.

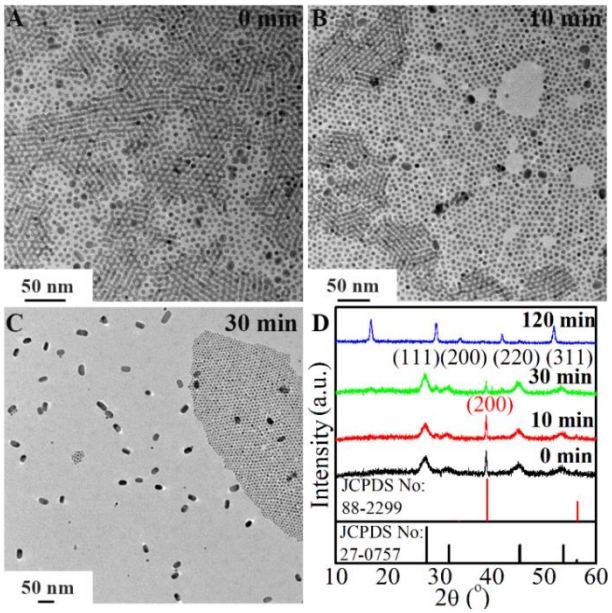

Fig. S5 (A-C) TEM images of $NaNdF_4$ nanocrystals obtained after different reaction times at 290 °C (A: 0 min, B: 10 min, and C: 30 min). (D) The corresponding XRD patterns (black: 0 min, red: 10 min, green: 30 min and blue: 120 min). The standard cards of cubic $NaNdF_4$ (JCPDS No: 27-0757) and cubic NaF (JCPDS No: 88-2299) are shown. Lattice planes are labeled using different font colors (black: cubic $NaNdF_4$ and red: cubic NaF). The XRD patters are normalized with respect to the most intense peak.

The growth mechanism of β-$NaNdF_4$ (x = 100%) nanorods is also investigated by recording the XRD patterns and TEM images for different reaction times at 290 °C (Fig. S5). Small α-$NaNdF_4$ nanoparticles (average diameter ~ 5.3 nm, JCPDS no. 27-0757) and NaF (JCPDS no. 88-2299) are obtained for reaction time t = 0 min (Fig. S5A and S5D and Fig. S6). For t = 10 min, both large (average diameter = 15.9 nm) and small (average diameter = 5.8 nm) nanoparticles are observed (Fig. S5B and Fig. S6); the former growing in size and becoming elongated with reaction time. For an example, for t = 30 min, apart from small nanoparticles (average diameter = 6.6 nm), nanorods with an average length = 24.4 nm and average width = 14.5 nm are obtained (Fig. S5C and Fig. S6). For both t = 10 and 30 min, β-$NaNdF_4$ nanocrystals coexist with their α–phase counterparts (Fig. S5D). Finally, for t = 120 min, only β-$NaNdF_4$ nanorods with an average length = 49.9 nm and average width = 27.4 nm are observed (Fig. 1D). It is therefore proposed that the growth of β-$NaNdF_4$ nanorods involves an Ostwald-ripening process with unstable α-$NaNdF_4$ nanoparticles

transforming to β-$NaNdF_4$ nanorods as the reaction progresses. It is worth mentioning that Yan *et al*. have previously demonstrated the presence of hexagonal NdF_3 during the initial stage of β-$NaNdF_4$ nanorod formation, which is not observed here.[4] A plausible explanation is the higher reaction temperature (330 ^oC) used in their study which caused the initially formed α-$NaNdF_4$ to undergo partial decomposition in the presence of oleic acid to form NdF_3: α-$NaNdF_4$ + oleic acid $\rightarrow$ NdF_3 + β-$NaNdF_4$ + Na-oleate + HF.[5]

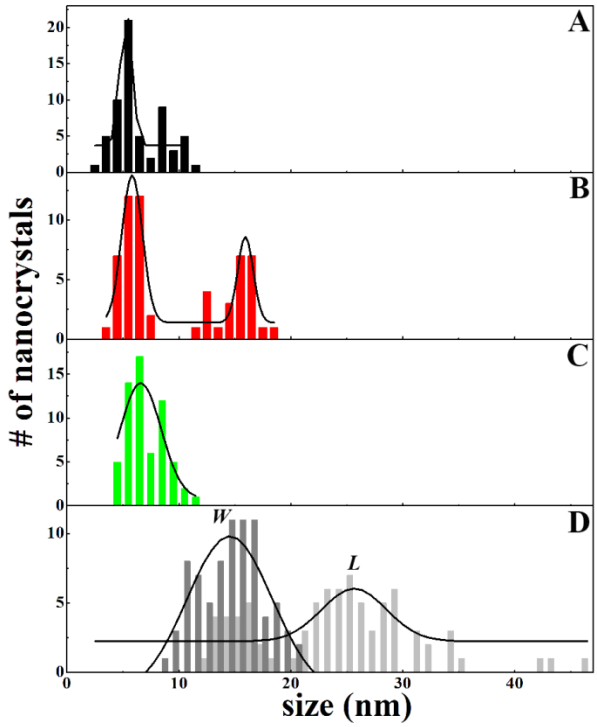

Fig. S6 Histograms of size distribution of $NaNdF_4$ nanocrystals obtained at 290 ^oC for different reaction times (A: 0 min, B: 10 min and C-D: 30 min). C refers to the spherical nanoparticles and D refers to the co-existing nanorods. The Gaussian fit in A gives the average diameters of nanocrystals for t = 0 min to be 5.3 $\pm$ 1.1 nm. The Gaussian fits in B give the average diameter of the groups of small and large nanoparticles formed for t = 10 min to be 5.8 $\pm$ 1.8 and 15.9 $\pm$ 1.4 nm, respectively. The Gaussian fit in C gives the average diameter of nanoparticles for t = 30 min to be 6.6 $\pm$ 2.2 nm, and the Gaussain fits in D give the average length (L) and width (W) of the nanorods to be 24.1 $\pm$ 2.9 nm and 14.5 $\pm$ 7.6 nm, respectively.

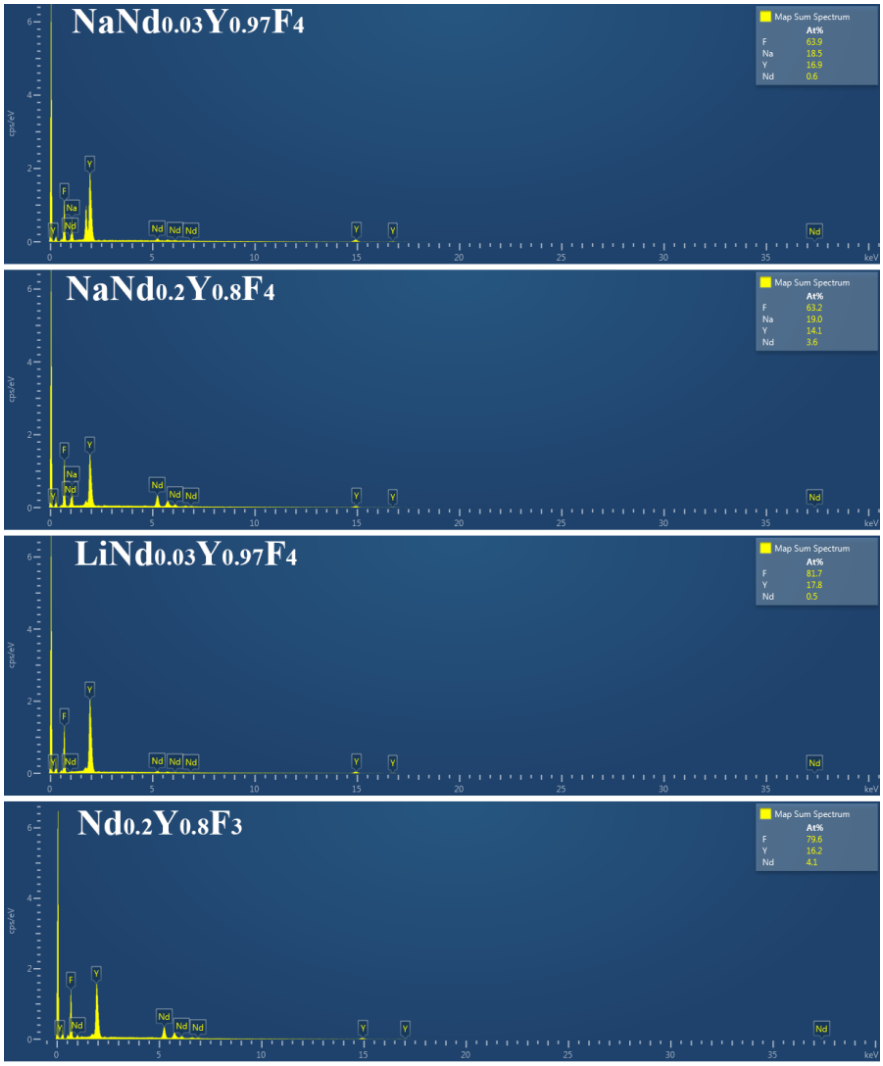

Fig. S7 Energy-dispersive X-ray (EDX) analysis results of $NaNd_{0.03}Y_{0.97}F_4$, $NaNd_{0.2}Y_{0.8}F_4$, $LiNd_{0.03}Y_{0.97}F_4$ and $Nd_{0.2}Y_{0.8}F_3$.

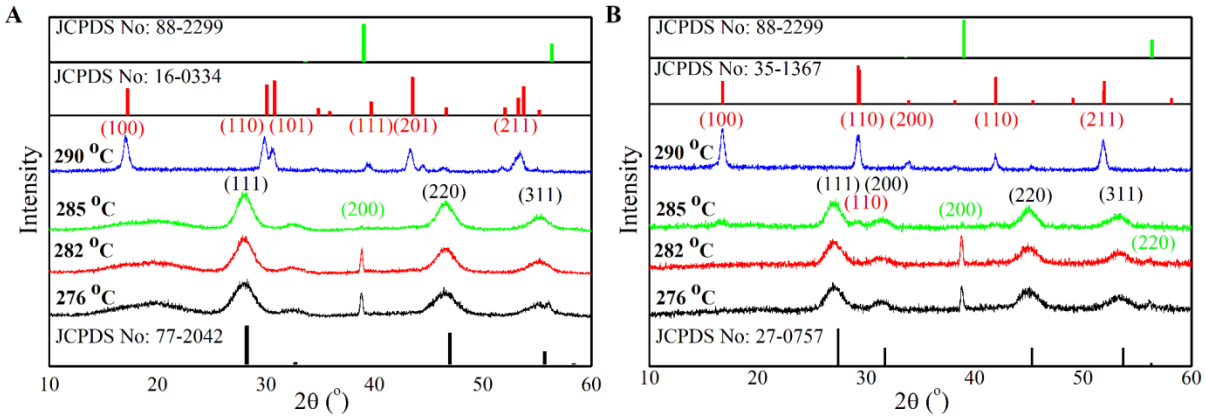

Fig. S8 XRD patterns of $NaNd_{0.03}Y_{0.97}F_4$ (A) and $NaNdF_4$ (B) for different reaction temperatures (T = 276, 282, 285 and 290 °C) and reaction time t = 2 h. The standard cards of cubic $NaYF_4$ (JCPDS No: 77-2042), hexagonal $NaYF_4$ (JCPDS No: 16-0334), cubic NaF (JCPDS No: 88-2299), cubic $NaNdF_4$ (JCPDS No: 27-0757) and hexagonal $NaNdF_4$ (JCPDS No: 35-1367) are also given. Lattice planes are labeled using different font colors (black: cubic $NaYF_4$ or $NaNdF_4$, red: hexagonal $NaYF_4$ or $NaNdF_4$ and green: cubic NaF).

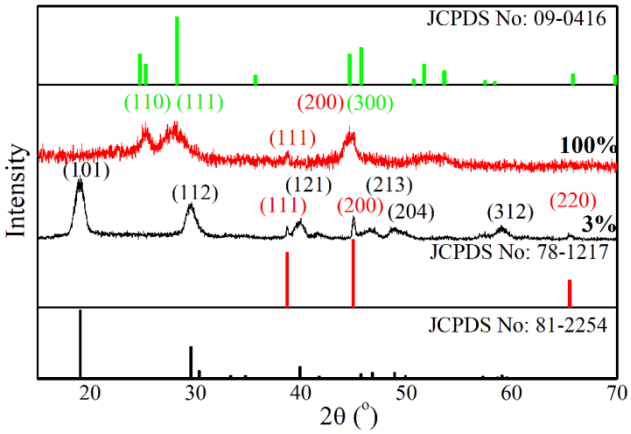

Fig. S9 XRD patterns of $LiNd_{0.03}Y_{0.97}F_4$ and NdF_3 obtained using 1.0 mmol LiOH. The standard cards of tetragonal $LiYF_4$ (JCPDS No: 81-2254), hexagonal NdF_3 (JCPDS No: 09-0416) and cubic LiF (JCPDS No: 78-1217) are given. Lattice planes are labeled using different font colors (black: tetragonal $LiYF_4$, red: LiF and green: hexagonal NdF_3).

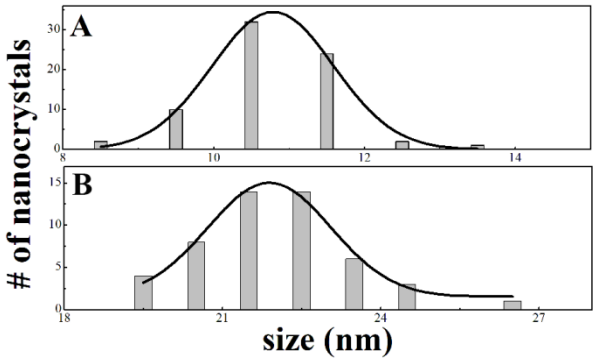

Fig. S10 Histograms of the size distribution of $LiNd_{0.03}Y_{0.97}F_4$ and NdF_3 nanoparticles for reaction time of 120 min. The Gaussian fits shown give the average diameters of $LiNd_{0.03}Y_{0.97}F_4$ and NdF_3 nanoparticles to be 10.8 ± 1.6 and 21.9 ± 2.3 nm, respectively.

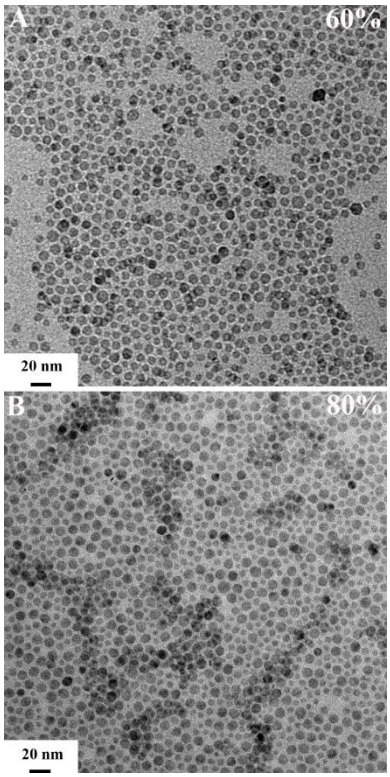

Fig. S11 TEM images of $Nd_{0.6}Y_{0.4}F_3$ (A) and $Nd_{0.8}Y_{0.2}F_3$ (B).

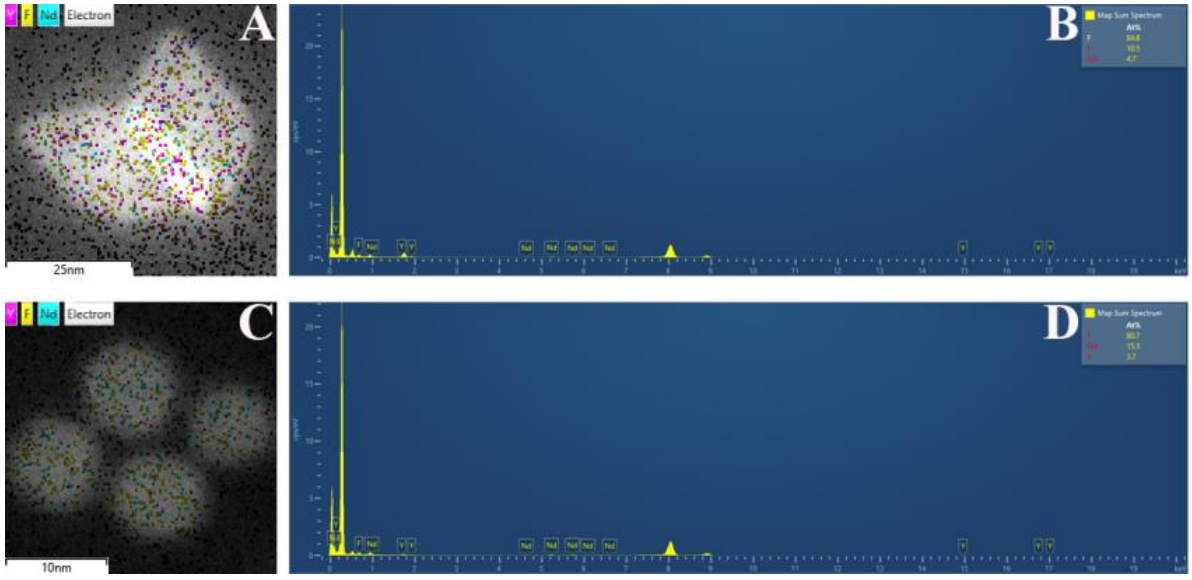

Fig. S12 HAADF-STEM-EDX images of parallelogram-shape nanocrystals (A) and spherical nanoparticles (C), and their corresponding EDX analysis results (B and D).

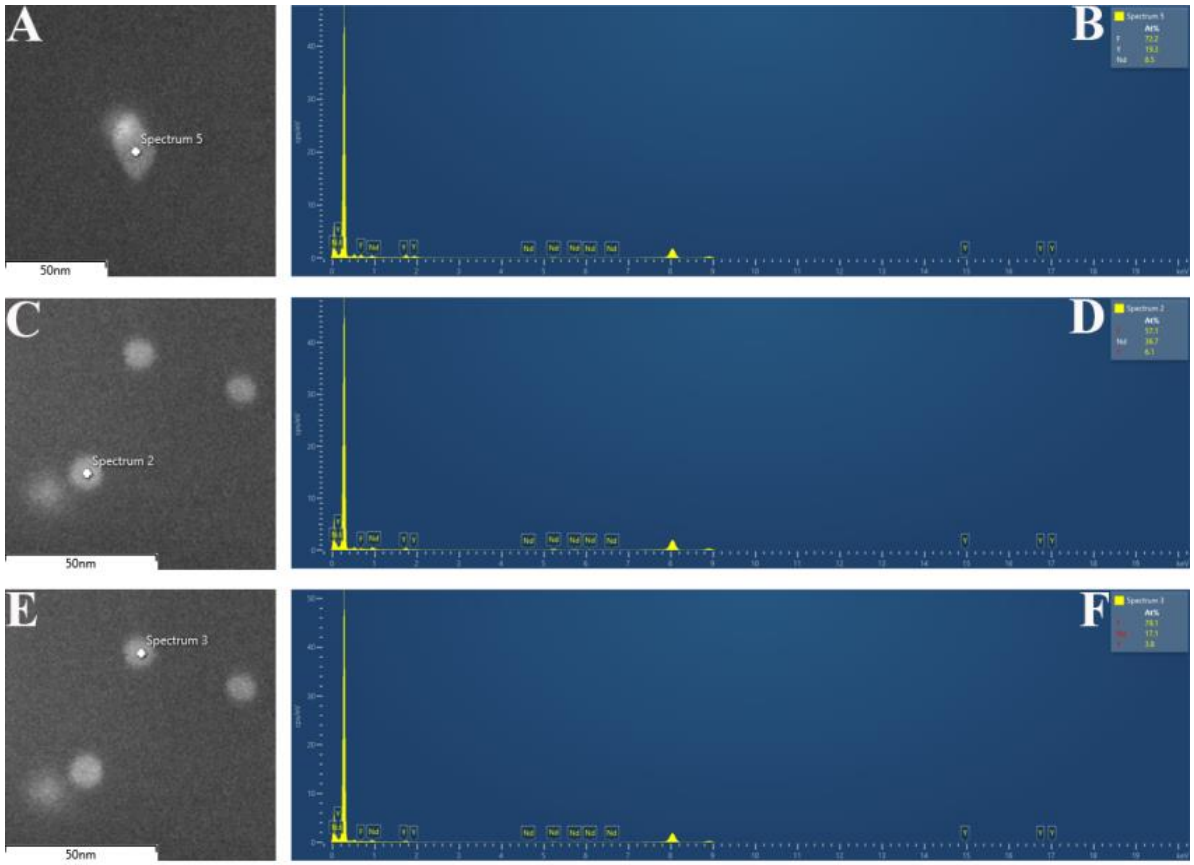

Fig. S13 HAADF-STEM images of parallelogram-shape nanocrystal (A) and spherical nanoparticles (C and E), and the EDX analysis results obtained from individual points (white dot) on the nanocrystals (B, D, and F).

Growth dynamics of $LiNd_xY_{1-x}F_4$ nanocrystals

The effect of reaction time is investigated next by performing time-dependent experiments. For x = 3% and t = 0 min, the TEM image shows several small nanoparticles (average diameter = 7.5 nm) (Fig. S14A and Fig. S15), and the corresponding XRD diffraction pattern reveals the co-existence of tetragonal Nd^{3+}-doped $LiYF_4$ nanocrystals, orthorhombic Nd^{3+}-doped YF_3 nanocrystals and LiF (Fig. S14C); likely formed *via* the following reactions:

$NH_4F + LiOH \rightarrow LiF + NH_3 + H_2O$

$(1 - x)Y(oleate)_3 + xNd(oleate)_3 + 3F^- \rightarrow Nd_xY_{1-x}F_3 + 3(oleate)^-$

$Nd_xY_{1-x}F_3 + LiF \rightarrow LiNd_xY_{1-x}F_4$

As the reaction progresses (*e.g.*, t = 30 and 120 min), the amounts of Nd^{3+}-doped YF_3 and LiF decrease and only diffraction peaks arising from Nd^{3+}-doped $LiYF_4$ are observed (Fig. S14C). The TEM image for t = 30 min (Fig. S14B) clearly displays both large (average diameter = 10.9 nm) and small nanocrystals (average diameter = 5.5 nm) (Fig. S15), whereas homogeneous $LiNd_{0.03}Y_{0.97}F_4$ nanoparticles (average diameter = 10.8 nm) are formed for t = 120 min (Fig. 2A). Therefore, Ostwald ripening is the mechanism governing the formation of tetragonal $LiNd_{0.03}Y_{0.97}F_4$ nanoparticles. Interestingly, we note that the average size of the large nanoparticles for t = 30 and 120 min are not significantly different (~ 10.9 nm). This suggests that the reaction is closed to completion at t = 30 min where the majority of the smaller sized Nd^{3+}-doped $LiYF_4$ nanocrystals have undergone dissolution to form the final product.

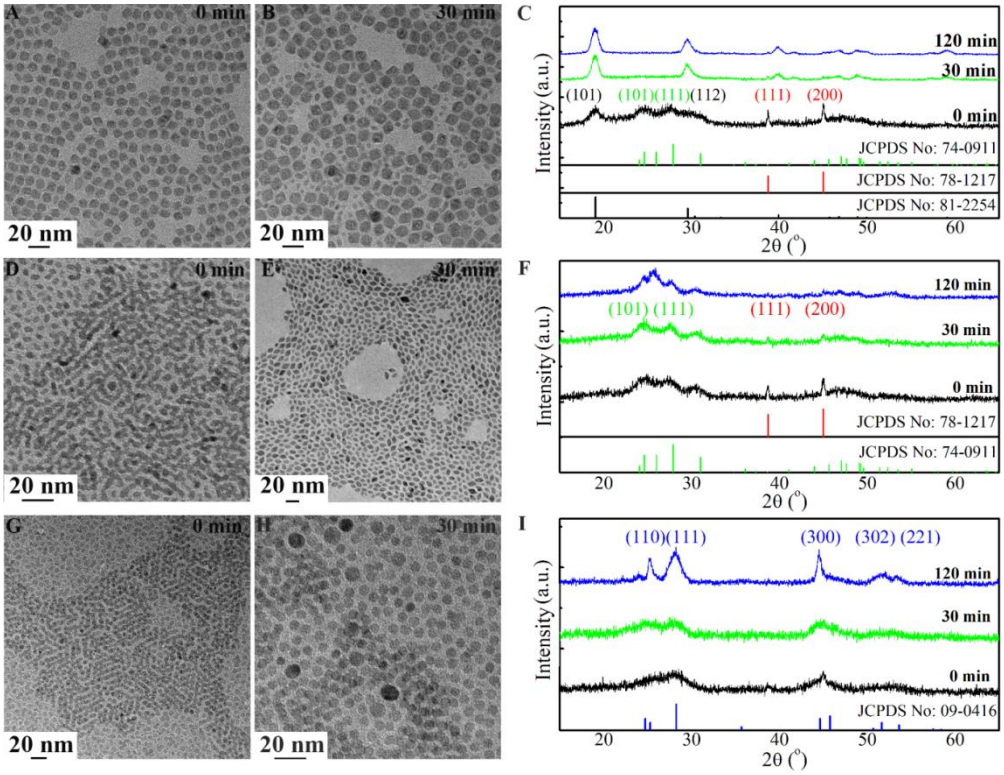

Fig. S14 TEM images of nanocrystals formed for different reaction times (t = 0 and 30 min) in the formation of $LiNd_{0.03}Y_{0.97}F_4$ (A, B) and $Nd_xY_{1-x}F_3$, x = 20% (D and E) and 100% (G and H). The corresponding XRD patterns for (A, B), (D, E) and (G, H) are given in C, F and I, respectively. The standard cards of tetragonal $LiYF_4$ (JCPDS No: 81-2254), cubic LiF (JCPDS No: 78-1217), orthorhormbic YF_3 (JCPDS No: 74-0911) and hexagonal NdF_3 (JCPDS No: 09-0416) are shown. Lattice planes are labeled using different font colors (black: tetragonal $LiYF_4$, red: cubic LiF, green: orthorhormbic YF_3 and blue: hexagonal NdF_3). The XRD patterns are normalized with respect to the most intense peak.

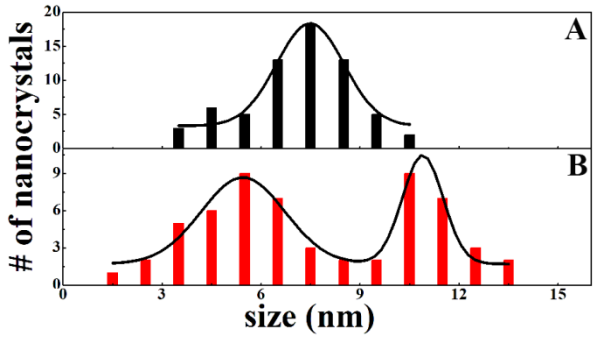

Fig. S15 Histograms of size distribution of $LiNd_{0.03}Y_{0.97}F_4$ nanocrystals at 290 °C for different reaction times (A: 0 min and B: 30 min). The Gaussian fit in A gives an average diameter of 7.5 ± 2.0 nm. The Gaussian fits in B give an average diameter of 5.5 ± 2.5 nm for the small nanoparticles and 10.9 ± 1.2 nm for the large nanoparticles.

For x = 20% and t = 0 min, small nanocrystals (average length = 4.8 nm) are initially formed (Fig. S14D and Fig. S16) which are attributed to orthorhombic Nd^{3+}-doped YF_3 (Fig. S14F). For t = 30 min, the diffraction peaks from LiF become weak (Fig. S14F) and both large (longest distance between opposite vertices L_l = 16.4 nm, Fig. S16) and small (L_l = 10.3 nm, Fig. S16) parallelogram-shape Nd^{3+}-doped YF_3 nanocrystals (*i.e.*, two groups) are visible in the TEM image (Fig. S14E). As the reaction progresses, the parallelogram-shape nanocrystals grow in size. For t = 120 min, two groups of parallelogram-shape orthorhombic $Nd_{0.2}Y_{0.8}F_3$ nanocrystals are also observed; one with L_l = 22.6 nm and the other with L_l = 13.3 nm (Fig. 2B and Fig. S16). The absence of dissolution of small nanocrystals suggests that Ostwald ripening is restricted here.[1] The nuclei are likely created at different times such that those formed at earlier times grow larger compared to the ones formed at later times.

For x = 100%, the initially formed hexagonal NdF_3 nanoparticles grow in size from 3.3 nm for t = 0 min to 6.4 and 21.9 nm for t = 30 and 120 min, respectively (Fig. S14G – S14I and Fig. S17). The growth of the NdF_3 nanoparticles after nucleation therefore proceeds by continuous deposition of existing precursors onto the crystals with reaction time.

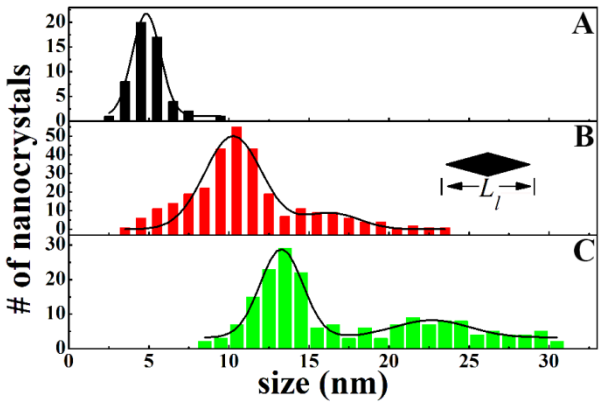

Fig. S16 Histograms of size distribution of $Nd_{0.2}Y_{0.8}F_3$ nanocrystals at 290 °C for different reaction times (A: 0 min, B: 30 min and C: 120 min). The Gaussian fit in A gives an average diameter of 4.8 ± 1.8 nm. The Gaussian fits in B give an average diameter of 10.3 ± 3.6 nm for the small nanoparticles and 16.4 ± 3.5 nm for the large nanoparticles. The Gaussian fits in C give an average diameter of 13.3 ± 2.7 nm for the small nanoparticles and 22.6 ± 4.7 nm for the large nanoparticles. L_l is the longest distance between opposite vertices.

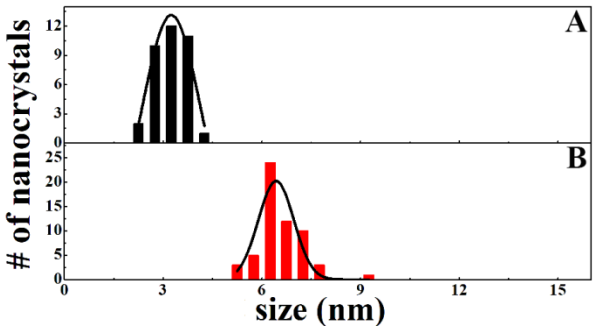

Fig. S17 Histograms of size distribution of NdF_3 nanocrystals obtained at 290 °C for different reaction times (A: 0 min and B: 30 min). The Gaussian fit in A gives an average diameter of 3.3 ± 1.8 nm, and the Gaussian fit in B gives an average diameter of 6.4 ± 1.1 nm.

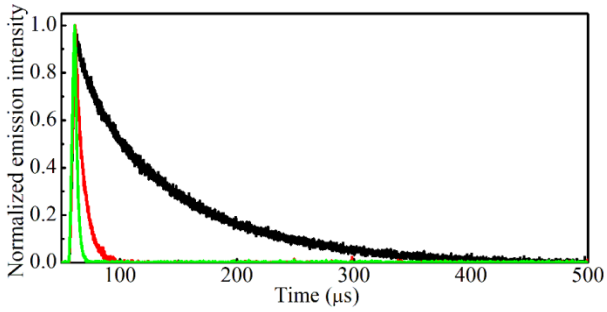

Fig. S18 Downconversion emission lifetime decay profiles of a chloroform solution of $NaNd_xY_{1-x}F_4$ nanocrystals (x = 3% (black), 20% (red) and 100% (green)). Excitation wavelength = 808 nm and emission wavelength = 875 nm.

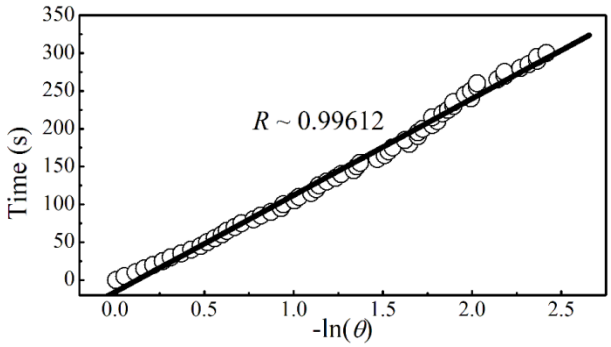

Fig. S19 Plot of the cooling time *vs*. -ln (θ) for $NaNdF_4$ nanorods in chloroform.

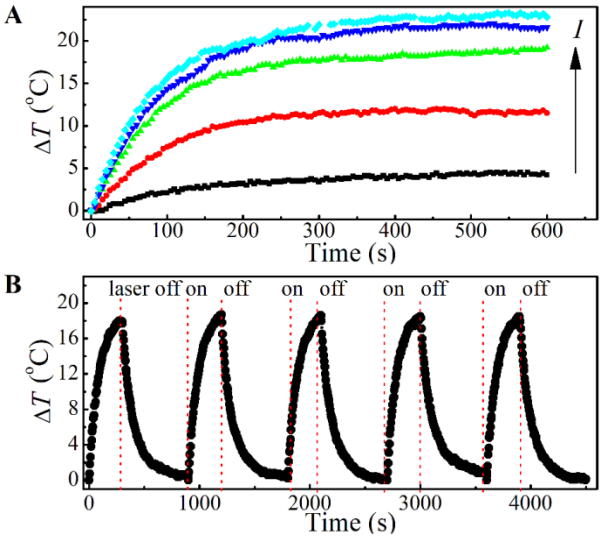

Fig. S20 (A) Time-resolved photothermal response profiles of a chloroform solution of $NaNdF_4$ nanorods excited using 808 nm laser with different power density (from bottom to top: 0.15, 0.66, 1.62, 2.20 and 2.60 W cm^{-2}). (B) Five cycles of temperature change profiles of a chloroform solution of $NaNdF_4$ nanocrystals excited using 808 nm laser (4.22 W cm^{-2}).

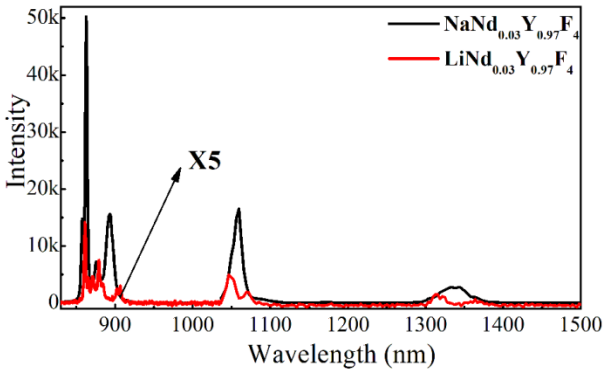

Fig. S21 Downconversion luminescence spectra of chloroform solutions containing separately $NaNd_{0.03}Y_{0.97}F_4$ and $LiNd_{0.03}Y_{0.97}F_4$ nanocrystals. The ratio of the QY of $NaNd_{0.03}Y_{0.97}F_4$ to $LiNd_{0.03}Y_{0.97}F_4$ for emission at ~ 1059 nm is 1:0.047. The excitation wavelength is 808 nm and the absorbances of the solutions at this wavelength are the same.

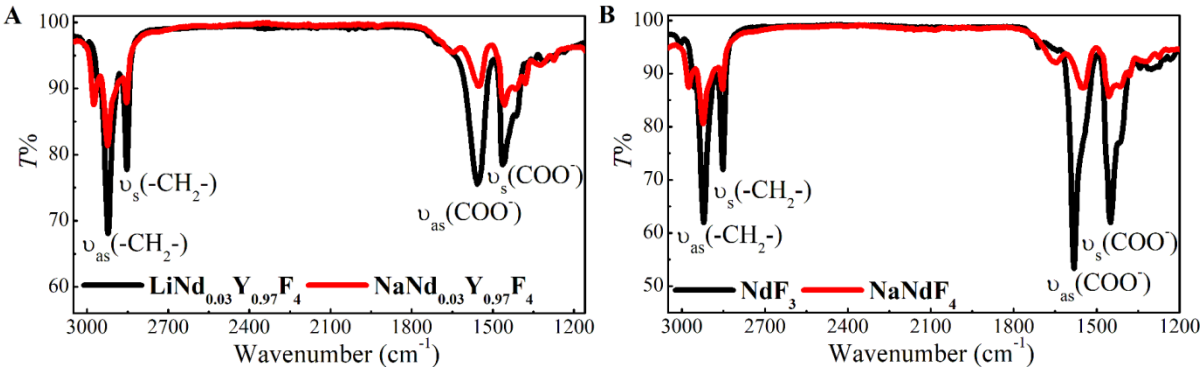

Fig. S22 ATR-FTIR spectra of (A) $LiNd_{0.03}Y_{0.97}F_4$ and $NaNd_{0.03}Y_{0.97}F_4$ nanocrystals and (B) NdF_3 and $NaNdF_4$ nanocrystals.

Fig. S23 Picture of the thermal imaging (left) and modified digital (right) cameras.

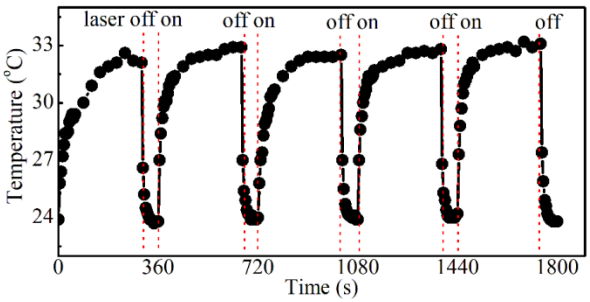

Fig. S24 Five cycles of temperature profiles of $NaNdF_4$ nanocrystals drop-cast on glass substrates excited using 808 nm laser (~ 1.8 W cm^{-2}).

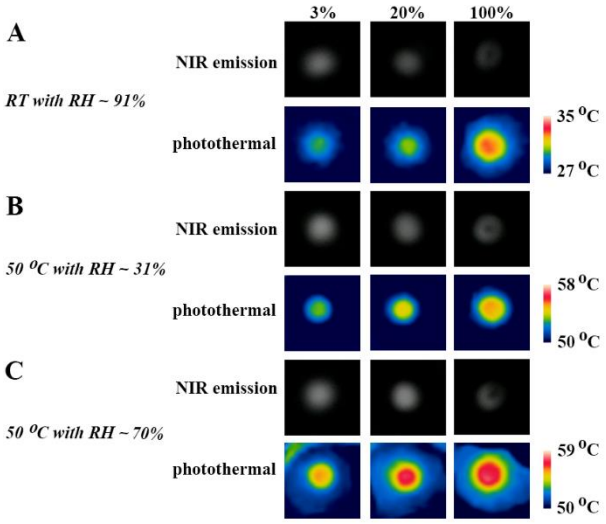

Fig. S25 NIR emission and photothermal images measured under different temperature (*T*) and humidity (RH) (A: *T* = 22 ºC/RH = 91 %, B: *T* = 50 ºC/RH = 31 % and C: *T* = 50 ºC/RH = 70%) of $NaNd_xY_{1-x}F_4$ (*x* = 3, 20 and 100 %) drop-cast on glass substrate.

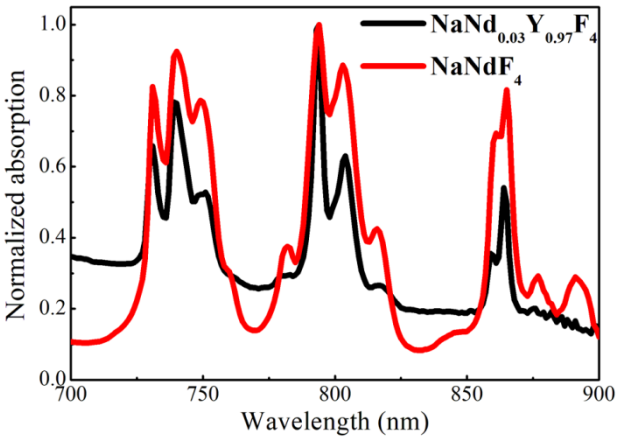

Fig. S26 Normalized diffuse reflectance UV-vis absorption spectra of $NaNd_{0.03}Y_{0.97}F_4$ and $NaNdF_4$ nanocrystal films on glass substrates. The spectra are normalized with respect to the most intense peak.

References

1. H.-X. Mai, Y.-W. Zhang, L.-D. Sun, C.-H. Yan, *J. Phys. Chem. C* 2007, **111**, 13730-13739.

2. J. Shan, Y. Ju, *Nanotechnology* 2009, **20**, 275603.

3. S. Wilhelm, M. Kaiser, C. Würth, J. Heiland, C. Carrillo-Carrion, V. Muhr, O.S. Wolfbeis, W. J. Parak, U. Resch-Genger, T. Hirsch, *Nanoscale* 2015, **7**, 1403-1410.

4. H.-X. Mai, Y.-W. Zhang, R. Si, Z.-G. Yan, L.-D. Sun, L.-P. You, C.-H. Yan, *J. Am. Chem. Soc.* 2006 **128**, 6426-6436.

5. A. N. Raj, T. Rinkel, M. Haase, *Chem. Mater*. 2014, **26**, 5689-5694.